JOURNAL OF APPLIED ELECTROCHEMISTRY 4 (1974) 249–257

Analysis of porous alkaline Cd-electrodes. I. Anodic high rate transients

PER SELÅNGER

Division of Chemical Technology, The Lund Institute of Technology, Chemical Centre, Lund, Sweden

Received 1 January 1974

Galvanostatic anodic high-rate transients in porous Cd-electrodes are analysed. A one-dimensional electrode model is developed. The model includes effects of variation in electrolyte composition and reaction surface activity. Overpotential transients are computed and compared with experimental transients. Failure in low porosity electrodes with great surface activity is in general caused by the blockage of pores at low rates. At high rates the discharge depth is limited by pure mass-transfer limitations. The reaction activity group i_0S is estimated from the experimental electrodes in conjunction with the model. Transition from pore blockage to pure mass-transfer limitations occurs between 100 and 200 mA cm^{-2} for a medium porosity of 0·60.

Nomenclature

Symbols

c electrolyte concentration, KOH, mol cm^{-3}
c_w solvent concentration, water, mol cm^{-3}
D diffusion coefficient, $cm^2\ s^{-1}$
f equivalents of extender on a Cd basis
F the Faraday equivalent, 96487 As per mol equiv.
g a density function for accessible surface activity; also the gravity constant, cm s^{-2}
i current density, A cm^{-2}
I current density, electrode load, A cm^{-2}
k_{bl} blockage constant for small pores, $cm^3\ A^{-1}$
l electrode thickness, cm
M mole weights
Q charge density, A min cm^{-3}
R universal gas constant 8·3143 J K^{-1} mol^{-1}
S surface activity, cm^2 per cm^3
t time, s
t_+^0 the transference number of the cation in the binary electrolyte with respect to the velocity of solvent.
v convective velocity, cm s^{-1}
$\bar{V}$ mole volume, $cm^3\ mol^{-1}$
x location co-ordinate inside the electrode, cm
y reaction extent related to total amount cadmium
z_+ the charge number of the cation in the binary electrolyte

Greek letters

α charge transfer coefficients $\beta F/RT$ and $(1\text{-}\beta)F/RT$, V^{-1}
β symmetry factor for charge transfer, = 0·5 was applied
ε porosity
ρ density, g cm^{-3}
κ conductivity, $ohm^{-1}\ cm^{-1}$ and permeability, cm^2
η overpotential, V
μ viscosity g $cm^{-1}\ s^{-1}$
ν stoichiometric coefficient
ν_+ number of cations into which a molecule of electrolyte dissociates

Subscripts

a anodic
c cathodic

Printed in Great Britain. © 1974 *Chapman and Hall Ltd.*

d diffusion
eff effective
i species i
o initial time distributions along the electrode co-ordinate x
p permeability
r electrolyte reactant
t charge transfer
1 solid phase
2 pore-electrolyte phase

1. Introduction

In this work a combination of experimental and theoretical work is carried out in order to gain experience from mathematical models as a means of analysing high rate electrodes.

The chief high-rate application of alkaline storage batteries is found in various engine cranking operations. A common property of batteries in heavy duty applications is the poor efficiency in the utilization of the active electrode material [1]. The materials used in electrodes are usually very expensive and this gives a rational motivation for an analysis to acquire a better background for making better electrodes in the future. The high-rate processes present a very complex problem and a performance analysis in general, should describe the overpotential transients at various load conditions. The load levels studied here are in the interval of 100–200 mA cm^{-2} and these levels draw attention to the important problem of mass transfer and current distributions within the porous electrodes. In the complete analysis the effects associated with structural changes arising from the precipitation of a solid product $Cd(OH)_2$ are also to be considered.

There have so far been very few integrated analyses [2–3] which reflect the usefulness of taking advantage of theoretical models in the analysis of experimental electrode transients. The analysis presented in this work is a method for the determination of parameters which are of importance for the simulation of commercial electrode systems and for their optimization.

2. Experimental

2.1. *Preparation*

Electrodes were prepared from dry mixtures of CdO and Fe_2O_3. The proportions were on a weight basis in the ratio 90:10. The mixtures were pressed into an electrode holder of plexiresin which defined a one-dimensional geometry, as the inside walls were electrically isolated. The electrode backing was made of machined rods of Ni metal. Through variation of the formation pressure it was possible to obtain different porosities. In the preparation of highly porous electrodes it was necessary to add finely divided KOH to the mixture to obtain a form-strength. The KOH was then leached out after a pre-reduction in a saturated KOH solution. The maximum porosity obtained by these methods was 0·85 and the minimum was 0·33. The electrode thickness varied from 0·7 to 2 mm. The electrode diameter was 10 mm.

During the formation cycles it was observed that the behaviour (i.e. reproducible discharges) of the electrodes became constant after 4 to 5 cycles. A pre-reduction for 48 h at 1 mA cm^{-2} was then followed by repetitive discharges and charges with the same current density for periods of 12 h. After a final conditioning, 24–28 h, the electrodes were ready for measurements at reproducible equilibrium potentials against a Hg|HgO cell in equal KOH concentration.

2.2. *Measurements*

All potential measurements were under galvanostatic conditions. The bulk electrolyte was stirred to eliminate the concentration potential error from the bulkside gradient. The overpotential at the working electrode was measured with a conventional Luggin-capillary connected to a reference-cell of Hg|HgO in the same electrolyte The polarizations were registered on a paper strip-recorder after compensation for the equilibrium potential.

The temperature during the various runs was $22 \pm 0{\cdot}5$°C and the electrolyte concentration varied between 4·5 and 5 M. The average porosities were determined by a volumetric neutralization titration procedure, combined with

electrode thickness measurements with a micrometer screw gauge. The mechanical volume was calculated from thickness data and the constructed electrode area. The electrolyte inside the electrodes was leached out with pure water. The leaching was repeated four times with pure water. The leached liquor was titrated with hydrochloric acid and related to the electrolyte volume inside the electrodes. The adherent electrolyte on the outer surface, was quickly washed away with water and thus excluded from the titration volume.

The charge distribution inside the electrodes was determined from microtome sectioned slices by chemical analysis. Sections with a thickness of 50 μm were analysed by the polarographic method for determination of the valence state distribution in the cadmium phase [4]. Only measurements of relative values between the metallic and the ionic states gave reliable results. The failure in the total value analysis was caused by the poor electrode strength, which produced only fractions of the sections under the microtome knife. The electrodes were embedded in a thin body of epoxy-resin and sliced under air-excluded conditions.

BET surface measurements were performed for some of the charged electrodes and for the ground materials. The cadmium oxide used was 5·0 $m^2\ g^{-1}$ and the ferric oxide was 8·8 $m^2\ g^{-1}$. Charged electrodes showed values from 1 $m^2\ g^{-1}$ to 2 $m^2\ g^{-1}$.

Permeabilities, were determined in an arrangement as shown in Fig. 1. The height of electrolyte h was measured at different time-points 1 and 2 for each electrode. The permeability was then calculated from

$$\mathscr{H}_p = \frac{\mu l}{\rho g(t_2 - t_1)} \ln \frac{h_1 - l}{h_2 - l}$$

which can be derived from Darcys law [10], taking into consideration that the whole pressure drop from the flow is within the electrode thickness l.

3. The electrode system

The solid phase is an interconnected cadmium matrix with a very high electrical conductivity

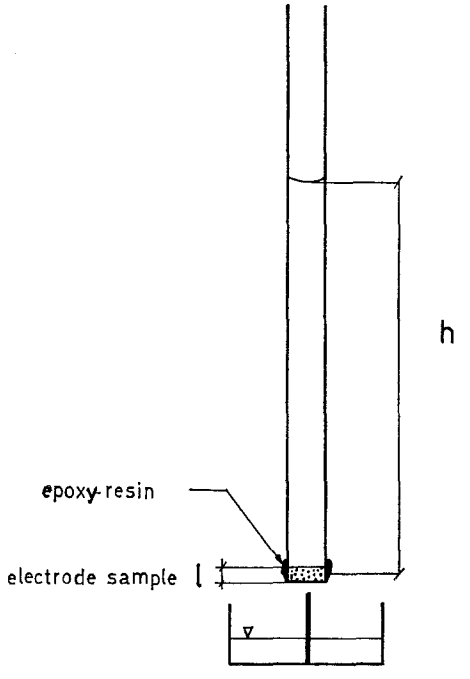

Fig. 1. The electrode permeability column.

solid phase consists of amorphous ferric oxide, which is used as a support. 80% of the metallic particles are in the size interval 0·1–1 μm; this was estimated with an electron microscope.

The electrolyte phase is considered as an interconnected electrolyte space in the fully charged state. The electrolyte space gradually decreases during discharge according to the positive net change in solid volume which occurs according to the Equation 1.

$$Cd(s) + 2\ OH^-(aq) \rightarrow Cd(OH)_2(s) + 2\ e^- \quad (1)$$

Basic assumptions made for a high-rate model for porous Cd-electrodes are as follows:

(1) The cadmium matrix is regarded as an iso-potential surface because of the high conductivity relative to the pore-electrolyte conductivity.

(2) The electrode system is regarded as a pseudo-homogeneous two-phase medium. The transport pathways for the species involved in the dissolution-precipitation reactions are regarded as small, compared to the reaction zone within the pore mouth region where the highest reaction current rate initially appears.

(3) The electrode system is regarded as a

in the full charged state. A minor part of the one-dimensional system according to the assumptions just made, and to the electrode design used in the experiments.

(4) Changes in ratio between liquid and solid volume due to precipitation of $Cd(OH)_2$ are described as quasi-compressible changes in the fixed co-ordinates of the pseudo-homogeneous electrode medium.

(5) The reaction product $Cu(OH)_2$ is assumed to be rapidly and completely precipitated.

(6) The transport equations for current and mass transports in the electrolyte phase are described by equations from the concentrated solution theory [5].

(7) The electrode is assumed to be isothermal which is confirmed by a check measurement at the current density of 0·2 A cm^{-2}. The temperature increased only 0·2°C during 4 min discharge under thermostatic experimental conditions. The approximation for isothermal conditions is thus within the total experimental error.

(8) The electrolyte gradient outside the electrode is eliminated by means of mechanical agitation.

(9) The time constant for charging the electrical double layer including the reaction transients is small and is of the maximum order of 100 ms for alkaline Cd electrodes. For most discharge transients of technical interest the effects mentioned can be neglected as controlling mechanisms in porous electrodes.

(10) The convection of electrolyte in the electrodes is due to the changing porosity.

(11) The changes in water concentration are relatively small and concentration profiles can be interpolated from electrolyte concentration density relationships.

4. Model equations

During deep discharges or for any thick electrodes it is necessary to include the ohmic polarization in the solid phase. In both these cases the ohmic polarization can be obtained from Equation 2

$$i_1 = -\kappa_1 \frac{d\eta_1}{dx} \tag{2}$$

The ohmic drop within the solid phase is neglected in this work according to the concept of an iso-potential matrix surface.

Thus, in this work η_1 is considered as zero inside the electrode.

The change in concentration of the binary electrolyte, KOH(aq), is obtained by integration of the one-dimensional simplified version of the general equation for the conservation of the electrolyte (Equation 3).

$$\frac{\partial c}{\partial t} + \nabla \cdot (cv) = \nabla \cdot \left[D\left(1 - \frac{d \ln c_w}{d \ln c}\right) \nabla c \right] - \frac{i \cdot \nabla t_+^0}{z_+ \nu_+ F} + \frac{\nu_r}{nF} \nabla \cdot i \tag{3}$$

The derivation of Equation 3 in this form is clearly presented and defined by Newman [5] and is extended here with a source term. Transport mechanisms included in Equation 3 are convection, diffusion and ionic migration. Convection and migration are often neglected beside the source and diffusion terms in low rate models. Migration is a minor term in the chosen transport representation, as t_+^0 has a very low concentration dependence $\nabla t_+^0 \approx 0$ [6] and it s therefore neglected in this high rate-model.

The convection term for the one-dimensional representation is of the form

$$\nabla \cdot (cv) = v \frac{dc}{dx} + c \frac{dv}{dx} \tag{4}$$

when the compressible property of the electrolyte space $\nabla . v \neq 0$ is taken into consideration.

The velocity v is calculated from the continuity equation for electrolyte flow (Equation 5)

$$\frac{\partial v}{\partial x} = -\frac{\partial \varepsilon}{\partial t} \tag{5}$$

Equation 5 is thus consistent with the assumptions made above, regarding the flow in the pore electrolyte. The local changes in porosity are obtained from

$$\frac{d\varepsilon}{dt} = \frac{1}{nF} \Delta \bar{V} \frac{di_2}{dx} \tag{6}$$

Combination of the Equations 5 and 6 gives the differential equation for v,

$$\frac{dv}{dx} = -\frac{\Delta\bar{V}}{nF}\frac{di_2}{dx} \tag{7}$$

which is to be integrated simultaneously with the transport Equation 8.

The simplified version of the Equation 3 for the one-dimensional case and with the effective coefficient of diffusion, $D_{eff} = D\varepsilon^{3/2}$ [11], introduced is

$$\frac{\partial c}{\partial t} = D_{eff}\left(1 - \frac{d\ln c_w}{d\ln c}\right)\frac{d^2c}{dx^2} - v\frac{dc}{dx} - c\frac{dv}{dx} \qquad \frac{v_r}{nF}\frac{di_2}{dx} \tag{8}$$

The source term in Equation 8 is assumed to be of the form given in Equation 9.

$$\frac{v_r}{nF}\frac{di_2}{dx} = \frac{v_r}{nF} i_0 S\, g(x)(1-\varepsilon)(1-u) \left[\left(\frac{c}{c_0}\right)\exp(\alpha_a\eta_t) - \exp(-\alpha_c\eta_t)\right] \tag{9}$$

A black-box experimentation with this porous electrode model in conjunction with a study of the steady state kinetics on plane Cd-surfaces has given the result shown. The kinetics on Cd-surfaces are still a challenging area for scientific exploration and the situation has recently been reviewed by Dunning *et al.* [2].

The exchange current density i_0 is related here to the bulk concentration c_0 of the electrolyte and S is the surface activity in cm^2 per cm^3. A density function $g(x)$ associated with S is introduced to describe the metallic Cd-distribution. The factor (1-u) gives the fraction of the electrode surface which contributes to the current. The variable u is assumed to describe the fraction of pores which will become inactive when the smallest pores cease to function because of their inefficient mass transport ability. For growing local rates, $\partial i/\partial x$, u is growing according to Equation 10.

$$u = k_{bl}\frac{\partial i}{\partial x}\cdot\frac{1}{\varepsilon^{0.5}} \tag{10}$$

The factor $1/\varepsilon^{0.5}$ is assumed to account for a varying quality in the distribution of interconnected pores for electrodes with different initial porosities. The effect of u is shown later. The exponent 0·5 is an empirical determination.

The electrode porosity, ε, is treated as a location- and time-dependent state variable. The stoichiometry determines the shift in ε, when applying Faraday's law to differences in mole volumes among solid reactants and reaction products.

The porosity is calculated locally as

$$\varepsilon = 1 - \frac{(1-\varepsilon_0)[(1-y)\bar{V}_1 + y\bar{V}_3 + f\bar{V}_4]}{(1-y_0)\bar{V}_1 + y_0\bar{V}_3 + f\bar{V}_4} \tag{11}$$

ε_0 is the initial porosity distribution. The extent of reaction y, is related to the theoretical capacity Q in the differential Equation 12. y_0 is the initial reaction extent. The solid components in Equation 11 are 1 Cd, 3 $Cd(OH)_2$, 4 Fe_2O_3.

$$\frac{dy}{dx} = \frac{\int_0^t \frac{di}{dx}}{Q} \tag{12}$$

The changes in surface activity are described as local changes in the g-function (Equation 13)

$$g(x) = g_0(x) - (y(x))^p \tag{13}$$

The exponent p has been recently interpretated by Dunning *et al.* [2] to be a structure-dependent parameter.

$\bar{V}_i$ is the mole volume of each solid component The factor f expresses the moles of the extender Fe_2O_3 on a cadmium basis.

The ohmic polarization within the electrolyte is obtained and described according to Equation 14, which is an approximation with regard to the concentrated solution theory [5]

$$i_2 = -\kappa_2\frac{d\eta_2}{dx} \tag{14}$$

The current density i_2 in the pore electrolyte phase is obtained from

$$\varepsilon\cdot\frac{di_2}{dx} = i_0 S\, g(x)(1-\varepsilon)(1-u) \left[\left(\frac{c}{c_0}\right)\exp(\alpha_a\eta_t) - \exp(-\alpha_c\eta_t)\right] \tag{15}$$

Concentration potentials are obtained from the Nernst equation (Equation 16)

$$\eta_d = \frac{RT}{nF}\ln\frac{a_1}{a_2} \tag{16}$$

In Equation 16 a_1, the electrolyte activity, is at a reference position outside the electrode and a_2 is the activity at any solution location inside the electrode. Accurate data for KOH (aq) is available in the literature [7].

The various overpotentials are treated analogously to a recently published work by R. Alkire [8]. The total and measured overpotential after compensation for the equilibrium potential is η and is composed as shown in Equation 17.

$$\eta = \eta_1 + \eta_2 + \eta_d + \eta_t \qquad (17)$$

where η_1 and η_2 are obtained from integral solutions to Equations 2 and 14 respectively. The charge transfer overpotential, η_t, profile is obtained from Equation 18 as differences based on iterative searches made on the total overpotential η and calculated η_1, η_2 and η_d profiles

$$\eta_t(x) = \eta - (\eta_1(x) + \eta_2(x) + \eta_d(x)) \qquad (18)$$

5. Boundary conditions

At $x=0$, $i_2 = I/\varepsilon$, $c = c_0$ the pore mouth conditions At $x=1$, the collector conditions are,

$$i_1 = I/(1-\varepsilon),\ i_2 = 0,\ \frac{dc}{dx} = 0,\ \frac{dv}{dx} = 0 \qquad (20)$$

The initial conditions for the state variables c, g, ε and y correspond to the initial-time distributions. For a gradient free electrode-electrolyte

$$c(x,0) = c_0 \qquad 0 \leqslant x \leqslant 1 \qquad (21)$$

is valid. The surface density function g varies from electrode to electrode and has the form

$$g(x,0) = g_0 \qquad 0 \leqslant x \leqslant 1 \qquad (22)$$

The porosity distribution is assumed to be uniform,

$$\varepsilon(x,0) = \varepsilon_0 \qquad 0 \leqslant x \leqslant 1 \qquad (23)$$

The reaction extent y is initially zero along the electrode

$$y(x,0) = y_0 = 0 \qquad 0 \leqslant x \leqslant 1 \qquad (24)$$

6. Results and discussion

Typical overpotential transients and their simulations for an electrode with $\varepsilon_0 = 0{\cdot}414$ in 4·45 M electrolyte are shown in Fig. 2. The best agreement between simulated and experimental transients was obtained for porosities over 0·40.

The charge distribution is shown in Fig. 3, where two examples from the analysed initial profiles are shown. In the estimations $i_0 S(1-\varepsilon)$, experimental charge distributions similar to those in Fig. 3 were applied in a curve-smoothed form. The curve-smoothed relation corresponds to the initial distribution g_0 in Equation 9.

Fig. 4 shows the computer estimated values of the parameter group $i_0 S(1-\varepsilon)$ as a function of the initial porosity. The estimates are based on short-time data, which means 1–2 s after switching on the constant current. The best

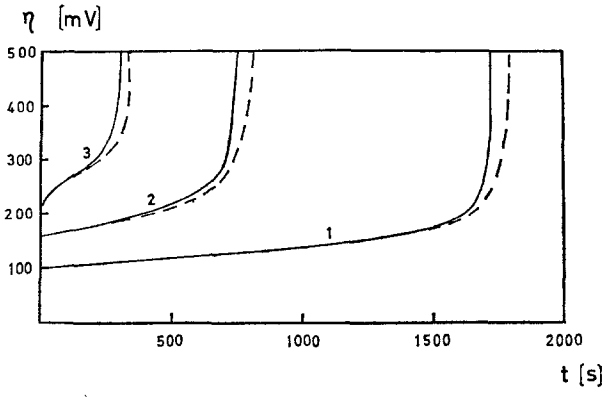

Fig. 2. Simulated and experimental curves for a typical electrode with an initial porosity $\varepsilon_0 = 0{\cdot}47$ and the thickness $l = 0{\cdot}152$ cm. The current density is 100, 150 and 200 mA cm^{-2} for curves 1, 2 and 3 respectively. Dotted curves are computer simulated transients.

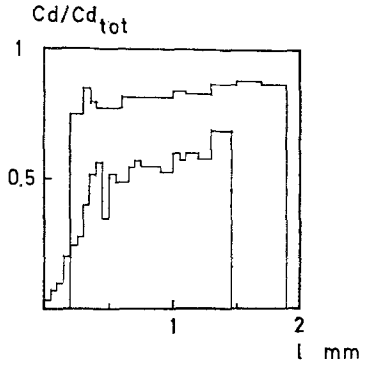

Fig. 3. Two typical initial charge distributions from the electrode sectioned analysis. The backwall coordinate is at electrode thickness l. The almost homogeneously charged electrode has the porosity $\varepsilon = 0{\cdot}72$ and the second electrode is a typical low porosity electrode with $\varepsilon = 0{\cdot}42$.

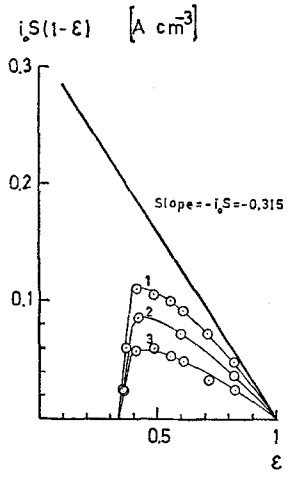

Fig. 4. The electrode activity $i_0S(1-\varepsilon)$ as a function of the porosity in the fully charged state. Curves 1, 2 and 3 represent the experimental values for the constant discharge current densities 100, 150 and 200 mA cm^{-2}. The straight line corresponds to the zero current limit, where u→0 when i→0, in the expression $i_0S(1-\varepsilon)$ $(1-u)$.

reproducibility was obtained for high porosity electrodes, which also were the more homogeneously charged electrodes.

The straight line drawn in Fig. 4 has the slope-i_0S. For the electrodes examined in this work i_0S was determined as 0·315 A cm^{-3}. The curves show the current density influence on the estimated available surface activity i_0S $(1-\varepsilon)$ before the introduction of the load dependent variable u. It may be of importance to point out that i_0S can be dependent on the preparation, and on the precision of the selected g-profiles. The amount of extender and possible binding materials, which are the usual components in commercial electrodes, can also be of importance. The electrodes in this work are all of the same composition and prepared with the uniform procedure described above. The constant $k_{bl}=0{\cdot}42$ was found from a least square analysis applied to Equation 10.

Low porosity electrodes gave large deviations from the relation $i_0S(1-\varepsilon)\cdot(1-u)$. The deviation from the last relation at porosities lower than 0·39 is interpretated as an effect of ineffectively interconnected electrolyte space which occurs in a region where the particles are closely packed. The specific current load in the residual pores thus increases the polarization at the expense of the ineffectively connected pores.

In general it is difficult to predict where the critical porosity limit appears and it can be expected to be dependent on the composition and structure of the active material. The observed limit is 0·35 which is for the electrode mixture examined in this work.

Fig. 5 shows high rate overpotentials at different time points as a function of the initial porosity for electrodes of comparable thickness.

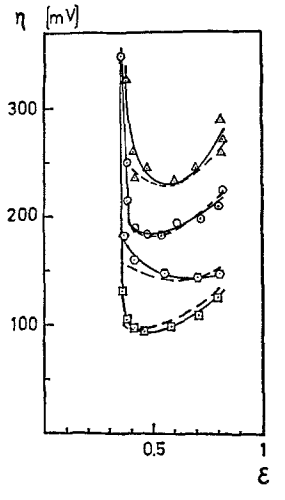

Fig. 5. Overpotentials at different time points for electrodes prepared with different porosities in the charged state. The electrode thickness is l = 0·160± 0·010 cm. Dotted curves are computer simulations. Experimental values are □ 20 s, 100 mA cm^{-2}; ⬭ 1200 s, 100 mA cm^{-2}; ○ 20 s, 200 mA cm^{-2} and △ 180 s, 200 mA cm^{-2}.

During short periods of time, polarization increases with increasing initial porosity. The explanation is that the electrode activity $i_0 S(1-\varepsilon)(1-u)$ decreases with increasing ε. The latter gives rise to an increasing internal surface load resulting in increasing polarization. At long discharges the electrodes will be exhausted, because of the insufficient transport of electrolyte from the bulk into the electrode inside.

Essentially two conditions define the exhausted state, reactant depletion from pure mass transfer limitations and precipitation of an insoluble reaction product $Cd(OH)_2$ causing restricted mass transfer.

For high rate cases, $i=200$ mA cm^{-2}, the concentration depletion is the controlling mode. This causes increasing ohmic and concentration polarizations together with a lowered reaction velocity. Low porosity electrodes are more sensitive to different load conditions than medium porosity electrodes because of the weaker transport abilities for both current and mass in the electrolyte phase. The larger reaction surface for low porosity electrodes does not compensate for the ineffective transport properties. The model predicts the general minimum polarization curve shape for varying porosity

Precipitation of the insoluble $Cd(OH)_2$ as a primary cause of polarization increase is obtained at lower discharge loads. Experiments performed at 100 mA cm^{-2} gave the latter polarization effects. The mechanism can be discribed as a continuous plugging of the pores in the pore mouth zone followed by an electrolyte depletion caused by the hindered mass transport This phenomena has recently been treated independently by Dunning [2] and Simonsson [3] and in this work their explanations are confirmed.

In order to test the arguments for the different exhausting mechanisms described above which were predicted in the model for various load levels, some electrolute permeability experiments were performed. Table 1 gives a comparison between two electrodes with almost identical physical properties. The electrodes were discharged to 500 mV final polarization. The permeabilities were measured according to the procedure described above.

Table 1 shows that the permeability at the final states is different for the two load levels. The κ_p value for the 100 mA cm^{-2} case together with the simulated final value of $\varepsilon_{\text{pore mouth}}$ indicates that this electrode is influenced by the precipitation of $Cd(OH)_2$ which is not the case for the other electrode at 200 mA cm^{-2}. The interval of 100–200 mA cm^{-2} seems to be a transition interval from pore blockage to pure mass-transfer limitations.

Table 1. Electrolyte permeabilities

I($mA\ cm^{-2}$)	$\kappa_p . 10^{10}\ cm^2$	ε_0	$\varepsilon_{\text{pore mouth}}$
100	0·32	0·53	0·36
200	1·15	0·51	0·45

The exponent p in Equation 13 is of general importance in the simulation of the experimental curves. In this work p has been found to fit the data best when $p=0{\cdot}80\pm0{\cdot}05$. The sensitivity of p increases with increasing current density. At $i=$ 100 mA cm^{-2} there was no significant difference between $p=1$ and $p=0{\cdot}80$ within the experimental error. At $i=200$ mA cm^2, ($p=0{\cdot}80$), p became a sensitive parameter. $p=1$ almost doubled the discharge time compared to $p=0{\cdot}80$ at $i=200$ mA cm^{-2}.

7. Solutions of equations

The solutions to the coupled Equations 7, 8 and 10–15 were obtained from an implicit finite-difference representation of the equations. These were iterated for the imposed constant current condition and for the given boundary conditions (Equations 19 to 24). A useful numerical method has been devised by Newman [9] which is suitable for treating complex coupled equations.

8. Conclusions

The model presented is based on rough simplifications concerning the microkinetical situation which is to be included in a more exact model. Another important extension to the model for general applications is to introduce the effects of pore size distributions which in this work are introduced empirically. The model gives a good

explanation of the influence of porosity on mass transfer and on surface activity for high-rate discharges, for the electrode mixture examined in this work.

Acknowledgements

The author wishes to thank Inge Fäldt for the introduction to electrochemistry and Sten Tore Lundin for his generous support while this work was being produced.

References

[1] S. U. Falk and A. J. Salkind, 'Alkaline Storage Batteries', Wiley (1969) pp. 466–78.
[2] J. Dunning, D. N. Bennion and J. Newman, *J. Electrochem. Soc.*, **120** (1973) 906.
[3] D. Simonsson, *J. Appl. Electrochem.*, **4** (1974) 109.
[4] P. Bro and H. Y. Kung, *J. Electrochem. Soc.*, **118** (1971) 519.
[5] J. Newman, 'Electrochemical Systems', Prentice Hall (1973) p. 242.
[6] S. Lengyel, J. Giber, G. Y. Beke and A. Vertes, *Acta Chim. Hung. Tomus*, **39** (1963) 357.
[7] G. C. Åkerlöf and P. Bender, *J. Am. Chem. Soc.*, **70** (1948) 2366.
[8] R. Alkire and A. Tvarusko, *J. Electrochem. Soc.*, **119** (1972) 340.
[9] J. Newman, *Ind. Eng. Chem. Fundamentals*, **7** (1968) 514.
[10] B. Bird, W. Stewart and E. Lightfoot, 'Transport Phenomena', Wiley (1960) p. 150.
[11] E. E. Petersen, 'Chemical Reaction Analysis', Prentice Hall (1965) p. 121.